Detection of Microtexture Regions in Titanium Turbine Engine Disks using Process Compensated Resonance Testing: A Modeling Study

Richard Livings[1, a)], Alex Mayes[1], Eric Biedermann[1], Julieanne Heffernan[1], Leanne Jauriqui[1], Siamack Mazdiyasni[2]

[1]*Vibrant corporation, Albuquerque, NM, USA*
[2]*Air Force Research Laboratory (AFLR/RXCA), Wright-Patterson AFB, OH, USA.*

[a)]Corresponding author: rlivings@vibrantndt.com

Abstract. Titanium alloys used by the aerospace industry, like Ti-64 or Ti-6242, with Microtexture Regions (MTR's) have been shown to exhibit significantly reduced dwell fatigue lifetimes. Over the last several decades, these titanium alloys have been used for critical components such as turbine engine disks, which are then susceptible to failure well below their expected service life. Current Nondestructive Inspection (NDE) methods are time consuming and can miss MTR's. Process Compensated Resonance Testing (PCRT) is a fast and accurate full-body NDE method that has been proposed for the detection of MTR's in titanium turbine engine disks. PCRT excites a part's resonance frequencies and correlates the resonance spectrum to the part's material and/or damage state. Turbine engine disks with MTR's will have different resonance spectra than fully isotropic disks. Both the MTR's geometric parameters (i.e. size, location, and orientation) and the microstructural parameters (i.e. degree of crystal alignment and orientation) will influence the magnitude and pattern of changes in the resonance spectrum. Using a Monte-Carlo approach, this work developed Finite Element Method (FEM) model population of disks with and without MTR's. These populations were analyzed to predict the effects of MTR parameter variation on resonance spectra and evaluate PCRT sensitivity to MTR's in the presence of normal geometric and material property variation. The feasibility of detecting MTR's in titanium turbine engine disks using PCRT methods is presented and discussed.

INTRODUCTION

Microtexture Regions (MTR's) in α-β phase titanium alloys (e.g. Ti-6V-4Al, aka: Ti64) are discrete regions of aligned α-crystallites that are generally ~0.1-10mm in size but can be as large as 10's of mm [1,2]. These clusters of aligned α-crystallites create localized regions of anisotropy in an otherwise isotropic material. The size, number, location, and degree of crystallite alignment (also called amount of microtexture) all influence the static and dynamic mechanical performance of a component. The presence of MTR's in safety critical aircraft components (gas turbine engine disks especially) is a topic of interest because MTR's can act as crack nucleation sites and significantly reduce dwell fatigue life. Several publications have explored the formation of MTR's and the underlying mechanisms of crack initiation from MTR's [1-10]. Based on these studies, the crystallite [0001] orientation most likely to result in a microcrack has been determined [1, 3]. Work is ongoing on the development of constitutive models that are capable of describing the role of processing (e.g. cooling rate, etc.) on MTR formation [8] as well as the role of microtexture parameters on the reduction of dwell fatigue lifetimes [9, 11]. One of the common methods for the detection of MTR's is ultrasonic backscatter. This method is subject to noise issues and requires trained technicians, multiple scan angles, and significant scan times. A full body inspection method, such as resonance, could drastically reduce the time required for inspection.

The presence of texture within a component will not only affect the static and dynamic mechanical performance but will also affect the component's resonance spectrum. This is true for both macrotexture, which transforms an isotropic component into a non-isotropic one, and microtexture, which behaves like an inclusion. The degree to which the resonance signature is modified by the presence of texture depends on the amount of texture (the degree of crystallite alignment) as well as the crystal orientation of the texture. In the case of MTR's, the sizes, locations, orientations, and numbers of MTR's will also affect the resonance signature. The use of resonance methods for the detection of MTR's has been proposed based on the known sensitivity of resonance methods to variance in the stiffness, discontinuities, and microstructure.

Process Compensated Resonance Testing (PCRT) is an objective, full-body NDE method that combines Resonant Ultrasound Spectroscopy (RUS) measurements with advanced statistical analyses to produce an automated Pass/Fail scan. More traditional RUS measurements can often miss damage/defects due to the masking effect of the material and geometric variations present within a population of components. PCRT was developed to overcome that limitation while maintaining comparable scan speeds (often less than 30 seconds for an entire part). Over the past two decades, PCRT has been shown to be capable of detecting a wide range of defects and damage [12, 13], has seen many commercial applications, specifically gas turbine engine hardware [14, 15], and has become a standard NDE method [16-18]. Recent developments in PCRT have focused on forward and inverse modeling of defects and material states as well as model trained PCRT Sorting Modules [19-24].

This paper presents the methodology to create FEM models of realistic MTR's in generic gas turbine engine disks as well as the capabilities of PCRT analyses in sorting components with MTR volumes from those without. The purpose of this work was to determine the sensitivity of resonance to the presence of realistic MTR volumes and examine the detectability of components with MTR's when the MTR signature was partially masked by benign material and geometry variations. Modeled populations were generated using Monte-Carlo style sampling, representative disk geometries, and realistic MTR parameters. The modeled resonance frequencies were then analyzed using pattern recognition and machine learning to determine a combination of resonances modes that were most indicative of MTR volumes. This work demonstrates the feasibility of detecting MTR's in populations of gas turbine engines disks using PCRT and lays down the groundwork for continued efforts in this vein.

MTR CHARACTERIZATION

The shape of an MTR is generally characterized as a prolate spheroid or a three-axis ellipsoid [25] as shown in FIGURE 1a. When describing the geometry and location of an MTR, it is useful to assign a local Cartesian coordinate system, ($\hat{e}_{MTR1}$, $\hat{e}_{MTR2}$, $\hat{e}_{MTR3}$). The coordinate system is aligned to the primary, secondary, and tertiary axes of the ellipsoid. An MTR's position within the disk model refers to the MTR centroid and is given based on the disk centric cylindrical coordinate system, ($\hat{e}_R$, $\hat{e}_\theta$, $\hat{e}_Z$), as shown in Fig. 1b. The orientation of the MTR is given with respect to the disk coordinate system and is described using a series of Euler rotations, (ϕ_1, ϕ_2, ϕ_3), as shown in Fig. 1c. Generally, the primary MTR axis is roughly aligned with the disk radial unit vector, $\hat{e}_R$, due to the forging process [25]. There is some amount of rotation about the transverse-horizontal and transverse-vertical directions, $\hat{e}_\theta$ and $\hat{e}_Z$, but this requires further characterization.

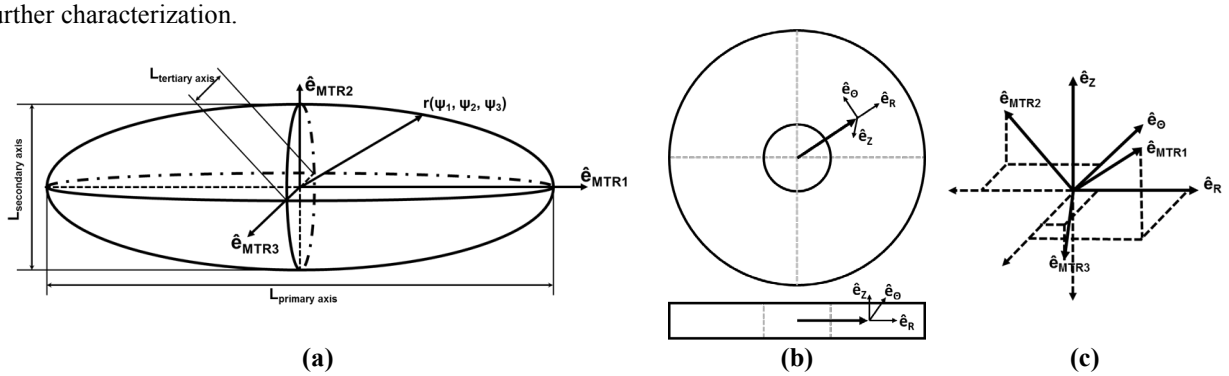

FIGURE 1. MTR diagrams showing (a) the triaxial ellipsoid geometry with MTR centric coordinate system, (b) location of MTR centroid in disk coordinates, and (c) orientation of the MTR with respect to the disk coordinate system.

The MTR model parameters used in this work were extracted from measured data in the form of Electron Backscatter Diffraction (EBSD) scans of titanium samples, henceforth referred to as "the Pilchak dataset" [1,2]. This

dataset includes four separate samples and images three orthogonal planes from each sample. Pilchak et al. (2016) processed the raw EBSD data to extract the parameters of the MTR's present in each sample. They used the open source Dream.3D program (BlueQuartz Software, Springboro, Ohio) along with a two-step improved burn algorithm. The extracted properties include: major (primary) axis length, minor (secondary) axis length, equivalent diameter, and inclination angle. As processed, the Pilchak dataset only provides information on the geometry and orientation of the MTR volumes. Both the ellipsoidal primary axis length and the primary to secondary aspect ratio parameters exhibit Weibull distributions as shown in Fig. 2. The inclination angle of the MTR's can give a general idea of the MTR orientation with respect to the forging direction but cannot provide the complete 3D orientation. MTR parameter probability density function (PDF's) were extracted from the Pilchak dataset by fitting three-parameter Weibull distribution functions to the axis length parameters and two-parameter Gaussian distribution to the inclination angle.

Variations in the forging and fabrication methodologies of titanium components can have a significant effect on the formation and characteristics of MTR volumes within the component. Pilchak et al. (2016) in particular have demonstrated that once an MTR is formed in a billet subsequent plastic deformation changes the geometry of the MTR volume, but not the texture [1, 2]. Thus, even though the Pilchak dataset is the most complete MTR characterization study to date, the MTR parameter PDF's used in this study are not necessarily representative of the MTR occurrence in a specific component or particular type of components.

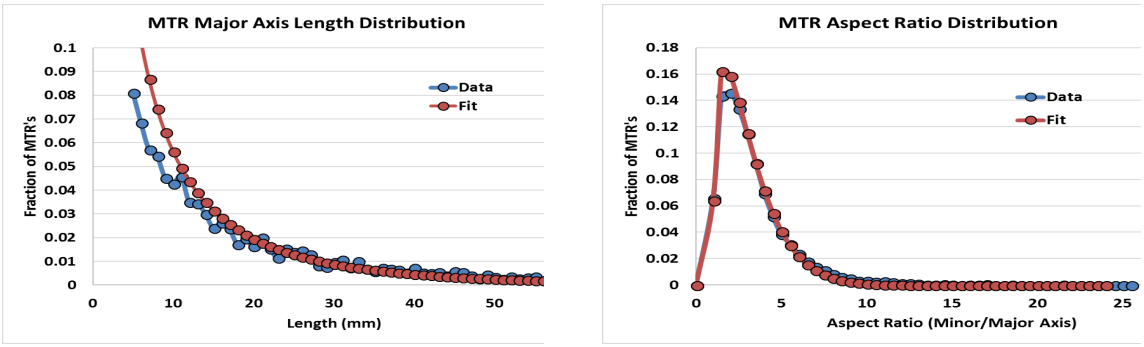

(a) **(b)**

FIGURE 2. Weibull distributions fit to the MTR dataset provided by Pilchak et al (2016) [1, 2] showing the (a) major axis length and (b) aspect ratio between the primary and secondary axis lengths.

As with any polycrystalline metallic sample, the material properties of an MTR are the Voight-Reuss (V-R) average of the individual phases and crystallites with respect to a given coordinate system. Unlike isotropic polycrystalline materials, in which the crystallites are randomly oriented, an MTR has aligned crystallites. As the similarity of the crystallite alignment increases the isotropy of the MTR decreases and the region behaves more and more like a single crystal. Yang & Turner (2007) [26] and Yang et al. (2012) [27] have proposed a microtexture parameter (based on the degree of misalignment of the α-crystallites) that can be used to quickly determine the V-R averaged elastic stiffness tensor of an MTR. Thus, the elastic properties of an MTR can readily be modeled from the crystallite orientation as measured from EBSD.

The primary focus of previous MTR studies has been on determining the underlying mechanism of the premature failure of titanium components. Little work has been done to characterize the MTR's themselves, especially in populations of components. There are several open questions that are limiting factors for this model-based study for MTR detection. What is lacking is better characterization, a good understanding of the statistical occurrence of MTR volumes in a given population of components, and a good understanding of the combination of MTR parameters that is most likely to lead to premature failure (severity metric).

MODELING

Disk Geometries

Two different aircraft gas turbine engine disk geometries were modeled and analyzed using the FEM software ANSYS 18.2 (ANSYS, Inc., Canonsburg, PA): a fan disk and a turbine disk. Fan disks are commonly made from a titanium alloy and are susceptible to the formation of MTR's. Turbine disks, on the other hand, are commonly made

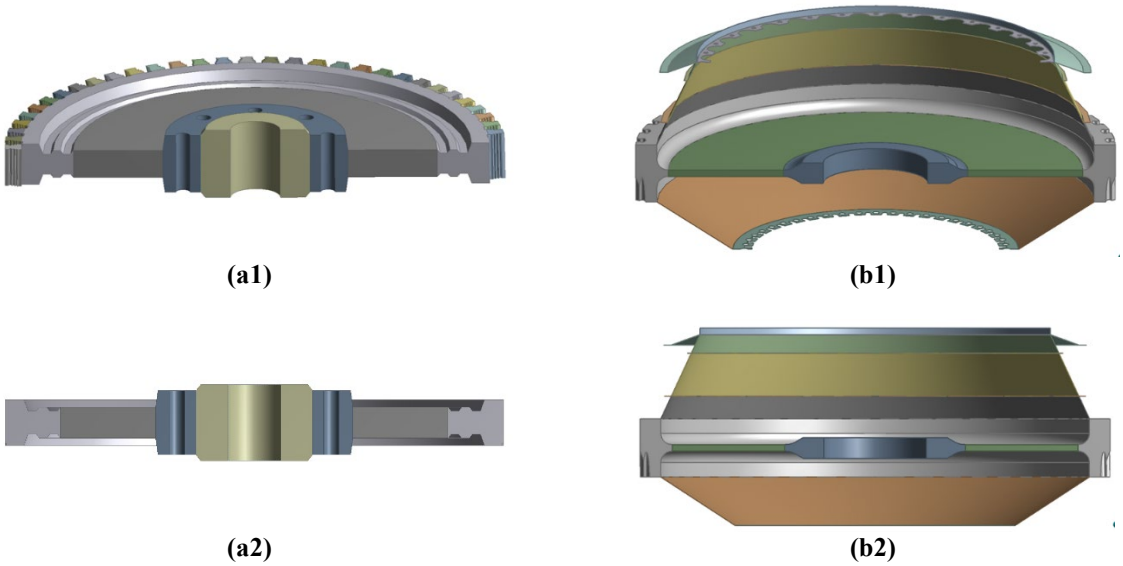

FIGURE 3. Turbine engine disk models used in this study showing (a) the generic turbine disk and (b) the generic fan disk.

from a nickel-based superalloy. A turbine disk geometry was included in this study to provide a different, thicker geometry for the evaluation of the sensitivity of resonance to the presence of MTR's. The fan disk geometry was a defeatured CAD model created based on measurements of a fan disk provided by AFRL. The turbine disk geometry came from an open-source CAD modeling archive [28] and was modified to make it more realistic. Changes were made based on measurements of various in-house turbine disks and include: the number of fir-tree slots, the bore-to-web thickness, and bore-to-edge thickness ratio. Fig. 3 shows the final geometries used in this study.

The mesh parameters for each model were selected to optimize computational resources, maintain feature fidelity, and give the most reasonable MTR resolution. To this end, the generic turbine disk was meshed entirely with 10-node tetrahedral elements, which had quadratic displacement behavior and approximate edge length of 5 mm, yielding a total of 480880 elements with 806123 nodes. The generic fan disk was divided into three mesh sections, the web, the flanges, and the bore & dovetails. A 20-node hex dominant mesh with edge length of 2.5mm was applied to the web section. The flanges were meshed with 8-node quadrilateral shell elements while the bore & dovetail sections were meshed with 10-node tetrahedral elements both of which had approximate edge lengths of 10mm. A total of 343,090 elements with 866,854 nodes were used for the generic fan disk geometry. For this model, MTR's were limited to the main disk and focused on the web section since they are unlikely to form in the flanges due to processing [25].

Microtexture Regions

MTR volumes for each model were generated by a script. The script inputs included: 1) part geometry, 2) MTR geometries, 3) ranges for MTR properties, 4) desired number or volume fraction of MTR's, and 5) penetration tolerances. MTR's were iteratively generated by randomly sampling the geometry and property distributions until a target MTR quantity or volume fraction was met. Penetration tolerance controlled whether the MTR's could penetrate the part surface and other MTR's during the generation process. The MTR geometry distributions were specified by the PDF's extracted from the Pilchak dataset [1, 2] discussed previously. MTR locations were random in the allowed sections while enforcing the penetration conditions. MTR orientations were generated via the likely alignment of the primary MTR axis with the radial unit vector (as specified by Pilchak [1, 2, 25]) with angular perturbations about the transverse-horizontal and transverse-vertical axes. The models used in this study employed normal distributions to account for these angular perturbations. Rotations were limited to ± 45° and ± 15° about the transverse-horizontal and transverse-vertical directions respectively.

Due to the drastic size differences between disks and the α-crystallite, the model elements were significantly larger than the crystallites. Therefore, for efficient use of computational resources, effective (or V-R average) elastic properties were assigned to the elements. The elements inside an MTR represent a cluster of partially to fully aligned α-crystallites, and as such, their effective elastic constants must be determined and applied. Elastic constants for each

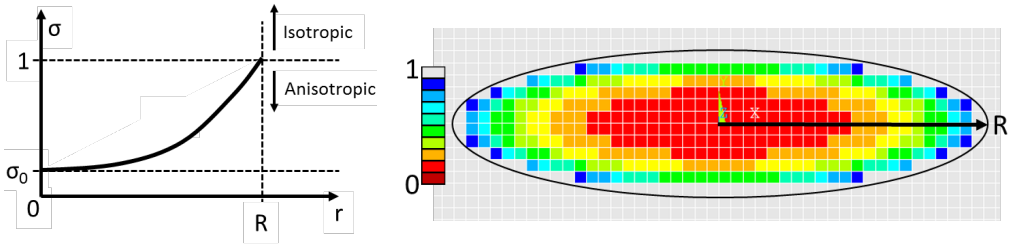

FIGURE 4. Diagram of the method for assigning elastic properties to the interior elements of a modeled MTR showing (a) the general trend of the texture parameter with MTR radius and (b) a graphical depiction of the texture parameter (σ).

MTR were calculated based on their microtexture parameter, as discussed previously. This work used the single crystal elastic stiffness constants from Simmons & Wang (1971) [29] in combination with the texture parameter given by Yang et al. (2012) [27] to calculate the elastic stiffness tensor.

MTR's are not discrete regions of constant texture, however; the most appropriate texture distribution model for the interior of an MTR is still an open question. In this project, the MTR was modeled as a textured region with a diffuse boundary. To account for this, the microtexture parameter was varied as a function of the MTR radial component, σ(R), such that the center of the MTR had the value σ_0, which is anisotropic, and the boundary of the MTR had $\sigma \geq 1$, which is isotropic. Each element within an MTR boundary was assigned a σ value with corresponding elastic constants based on the location of its centroid. Fig. 4 provides an illustration of assigning the σ values to the elements within an MTR. In this figure, red is the most anisotropic, blue the least, and grey is isotropic.

The α-crystallites that comprise an MTR are at least partially aligned to a Voight-Reuss averaged $[0001]_{VR}$ direction. The amount of misalignment from $[0001]_{VR}$ is described by the microtexture parameter, so the elemental coordinate system for each element within an MTR should have the same orientation. Alignment of the microtextured elastic stiffness tensor with the averaged crystallite coordinate system was accomplished by rotating the elemental coordinate systems. Note that the $[0001]_{VR}$ vector of an MTR is not necessarily coincident with the unit vector of the MTR primary ellipsoidal axis, or the other axes.

To create a modeled disk with realistic MTR volumes, the MTR volumes were generated and then placed into the existing mesh of the disk model. Modifying the existing mesh prevented the modification of the mesh structure and thus the epistemic modeling error due to mesh variations. This approach to generating MTR's within a disk volume allowed for the presence of a random number of MTR's with realistically random placements, geometries, and orientations.

The current method of inserting MTR volumes into a disk geometry was selected after considering the limitations of other approaches. There is a threshold on the number of nodes a model can have before the computational cost becomes impractical. Thus, with the method used in this study, the element size was the minimum MTR size that could be modeled. Smaller MTR volumes could be modeled at the expense of the freedom to place the MTR's randomly within the volume of the disk. If smaller MTR's were inserted at random locations, then the required local mesh refinement would increase the epistemic error. Alternatively, the MTR locations, geometries, and orientations could be kept consistent to eliminate the mesh variation, but then only the microtexture parameter and crystal orientation could be changed.

Monte-Carlo Design Space

Using the generic disk geometries and the MTR modeling method, Monte-Carlo (MC) design spaces were created to study the sensitivity of resonance frequencies to the presence of MTR's. This modeling procedure is described elsewhere [20, 21, 23]. Table 1 provides a summary of the parameters that were used in the creation of the MC space. The MC space for each geometry produced two distinct populations, nominal and MTR. The nominal population comprised components with acceptable processing variation only. In these models the processing variation included material properties (E, ν, and ρ) and the geometry (web thickness, slot width, bore hole diameter, bore hole position, bolt hole diameter, and bolt hole position), which were based on measurement uncertainty and machining tolerances respectively. The MTR population consisted of components that contained MTR volumes *in addition* to the processing variations. MTR parameters included location, number/volume fraction, geometry, MTR orientation, crystal orientation, and amount of texture. The realistic representation of MTR's included allowing randomized locations,

TABLE 1. Parameters, values, and ranges used in the Monte-Carlo studies of generic Ti64 turbine engine disks with realistic MTR's.

Param Type	Parameter	Nominal	Min	Max	Model	Sampling & Distribution
Material	**E (GPa)**	116.37	98.00%	102.00%	TD/FD	R-N
	ν	0.3192	98.00%	102.00%	TD/FD	R-N
	ρ (kg/m^3)	4620	99.80%	100.20%	TD/FD	R-N
Geometry	**Web Thickness Variation (cm)**	0	-0.00508	0.00508	TD/FD	R-N
	Slot Width (mm)	3.3	3.29	3.31	TD	R-N
	Bore Hole Diameter (cm)	7	6.9975	7.0305	TD/FD	R-SN
	Bore Hole Offset X (cm)	0	-0.013	0.013	TD/FD	R-N
	Bore Hole Offset Y (cm)	0	-0.013	0.013	TD/FD	R-N
	Bolt Hole Diameter (cm)	2	1.9975	2.0254	TD	R-SN
	Bolt Hole Offset R (cm)	0	-0.013	0.013	TD	R-N
MTR	**Location (R, Θ, Z)**	--	--	--	TD/FD	R-E
	Volume Fraction	--	0.50%	2.00%	TD/FD	E-4 Bins
	Major Axis (mm)	5	5	60	TD/FD	R-W
	Aspect Ratio	1	1	10	TD/FD	R-W
	Microtexture Parameter σ	--	1	0.0001	TD/FD	R-E
	MTR Orientation (φ1, φ2, φ3) (deg)	--	0	90	TD/FD	R-E
	Crystal Orientation ω (deg)	0	-45	45	TD/FD	R-N
	Crystal Orientation θ (deg)	45	0	90	TD/FD	R-N
	Crystal Orientation P (deg)	0	-45	45	TD/FD	R-N

TD – Generic turbine disk geometry **R** – Random sampling **E** – Even sampling or distribution **W** – Weibull distribution
FD – Generic fan disk geometry **N** – Normal distribution **SN** – Skew-normal distribution

randomized sizes, and random numbers of individual MTR's. The volume fraction of MTR's ranged between 0.5% and 2%, and MTR volumes were constrained to a minimum distance of 5mm from other MTR's and disk surfaces.

The MC parameters were used to generate 100 nominal and 50 MTR components for the generic turbine while the generic fan disk had 100 nominal and 59 MTR components. Since the generation of realistic MTR's was the intention of this study, this MC space did not prevent MTR's with near-isotropic properties ($\sigma>0.5$) or control the number of MTR's. MTR's with near-isotropic properties are very similar to the surrounding medium and were expected to be more difficult to detect. The potential design space was quite large due to the lack of information available in literature about the probability and structural impact of different MTR configurations. Additional knowledge about what is likely to occur and what is a performance risk can help constrain the design space and more effectively evaluate PCRT sensitivity. In this study the random parameter combination approach was considered the optimal modeling method with the available information.

ANALYSIS

Once the resonance frequencies were determined via modal analysis for each of the MC design points, the resonance responses to parameter variations were analyzed to identify resonance modes that were diagnostic of the presence of MTR's. FIGURE 5 shows a summary of the resonance frequencies from the MC spaces for the generic disk geometries and realistic MTR's. FIGURE 5 plots the mode dependent frequency averages (data points) and standard deviations (error bars) for the nominal (green) population and the MTR (orange) population. The maximum

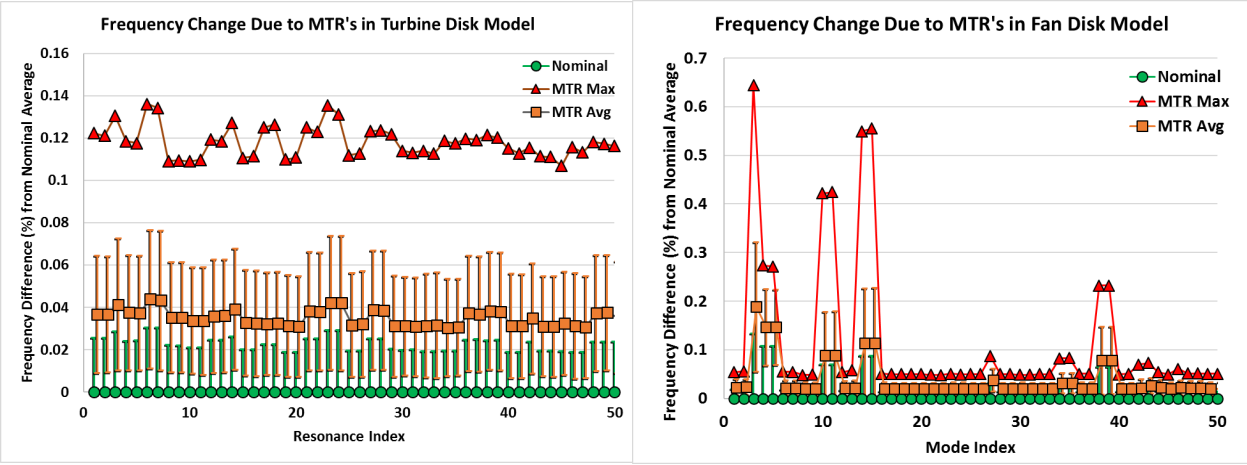

(a) **(b)**

FIGURE 5. Resonance frequency variation of the Monte-Carlo populations from baseline for (a) the generic turbine disk and (b) the generic fan disk. Error bars represent 1 standard deviation of the population.

frequency difference due to the presence of MTR's is also plotted. All quantities were normalized to the average of the nominal population for each mode. With this type of plot, the relative influence of defect/damage on the resonance frequencies can be determined with respect to the influence of the expected process variations present in a given population. Little to no overlap of the nominal and defective populations for three or more modes indicates that the defective parts can be sorted with a basic outlier screening. Some to significant overlap of the two populations requires a more complex approach, namely the application of the Vibrational Pattern Recognition (VIPR) algorithm described below.

In the case of both MC spaces, there was some overlap of the nominal and MTR populations, but the average of the MTR population was distinct from the nominal population and was slightly higher than the standard deviation of the nominal population. This indicated that the components with MTR's were likely detectable with a targeted sorting solution. Also noteworthy was the variation in the sensitivity of the resonance modes. For the generic turbine disk geometry (Fig. 5a) all of the modes seemed to be similarly sensitive to the presence of MTR's. The resonance modes of the generic fan disk, on the other hand, exhibited significant variance in sensitivity. This was due to the three sections of the fan disk (web, fore flange, and aft flange) vibrating individually. The least sensitive modes were those in which the flanges were vibrating while the most sensitive modes were those in which the web is the primary resonator, which is likely due to constraining the MTR's to the web section.

VIPR (Vibrant Corp. Albuquerque, USA) is a proprietary pattern recognition algorithm that was developed to target specific defects and determine the combination of resonance frequencies that is most diagnostic for the targeted condition and is now a standard analysis method [17, 18]. As with other machine learning applications, training sets (both nominal and defective) must be provided so that the algorithm can learn which resonance patterns are diagnostic. VIPR sorts nominal parts from defective parts using the Mahalanobis-Taguchi System (MTS) [30, 31] and bias discriminator. MTS is the magnitude of the difference vector between a given part and the central tendency of the nominal population. The bias discriminator is an n-dimensional surface separating the classifications (good/bad) when the population clouds are indistinct. A typical VIPR solution provides a scatter plot of x-y ordered pairs (Bias, MTS) for each part. Based on this approach, passing parts will have negative values in both Bias and MTS (quadrant III) while failing parts will have a positive value in the Bias, MTS, or both.

RESULTS AND DISCUSSION

VIPR algorithms were applied to the output frequencies MC populations for the generic gas turbine disk geometries to target parts with MTR's. The goal was to generate an objective Pass/Fail PCRT Sorting Module by identifying the optimal combination of resonance peaks that were most diagnostic of MTR's in a component. To this end, VIPR was trained to pass the components without MTR's (acceptable parts) while failing components with MTR's (unacceptable parts). In the training sets, the acceptable groups comprised components with nominal geometrical and material variations only. The unacceptable groups in the training sets comprised components with modeled

TABLE 2. Summary of targeted MTR sorts for generic disk geometries.

Model Geometry	Number of Parts in Training Set		Number of VIPR Peaks	Good Part Pass Rate	MTR Fail Rate
	Good Parts	MTR Parts			
Turbine Disk	100	50	7	97/100	44/50
Fan Disk	100	59	7	94/100	58/59

MTR's *in addition* to the geometrical and material variations present in the acceptable group. A summary of the VIPR sort for the two geometries is provided in Table 2.

The results of the VIPR sorts for the generic turbine disk and fan disk geometries are given in Fig. 6a and Fig. 6b respectively. In these plots, the parts in the bottom-left quadrant passed the sort and parts in the other three quadrants failed the sort either by MTS, Bias, or both. As described previously, the components with MTR's had a random number of MTR volumes (between 1 and 60) and each of these volumes had random locations, sizes, and properties. No correlative relationships were found between any single MTR parameter and the VIPR failure metrics, however, there was a common factor amongst the unacceptable parts that passed. These parts contained MTR volumes (either a single large volume or multiple small volumes) with low texture ($\sigma > 0.5$). This means that these MTR's were nearly isotropic and would have been nearly indistinguishable from the surrounding bulk material. The minimal discontinuity between these low texture MTR's and the bulk material would also imply a lower risk for crack nucleation and propagation, but additional research into severity metrics would be required to confirm this. The nominal parts that fail tend to have all of their parameters towards the higher ends of the distributions (Table 1).

Analysis of the generic turbine disk database yielded a seven-peak VIPR sorting solution targeting disks with MTR's. Based on the seven diagnostic resonance modes, 97% of the acceptable parts (nominal parameters) passed and 88% of components with MTR's failed this sort (shown graphically in Fig. 6a). A more conservative sort can be constructed that will fail all the components with MTR's at the expense of a higher fallout rate of the acceptable parts. Cross-validation of the current solution demonstrated that this sorting solution was robust, meaning any additional parts with moderate to high texture MTR's would have a high likelihood of detection. Analysis of the generic fan disk model database yielded similar results to the turbine disk. Seven resonance modes were identified by the VIPR analysis as the most diagnostic. Based on these diagnostic modes, 94% of acceptable parts (nominal parameters) passed the sort while 98% of the components with MTR's failed (shown in Fig. 6b). This sort had a higher MTR detection rate at the expense of a higher acceptable part fallout rate when compared to the turbine disk sort.

Although the targeted defect analysis of these two geometries proved successful, these were generic geometries. That, combined with the low availability of gas turbine disks and the difficulty in detecting MTR's, means that these sorts could not be subjected to field testing. This does, however, serve as a proof of concept for future work into the detection of MTR's in titanium components using PCRT methods. Note that a PCRT scan of the diagnostic peaks would take less than 30 seconds whereas an ultrasonic scan would take more than several hours.

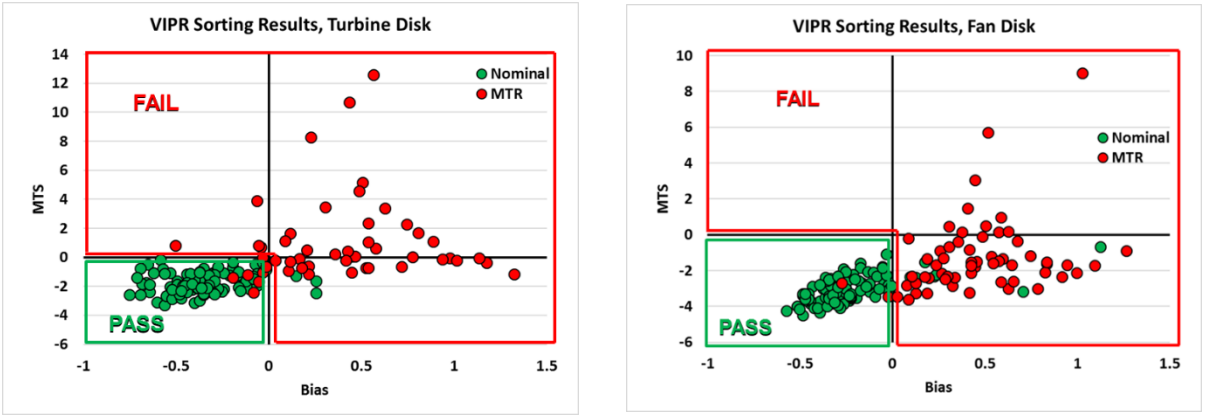

(a) **(b)**

FIGURE 6. VIPR solutions for targeting MTR's in generic modeled disk geometries for (a) turbine disk and (b) fan disk. Passing parts will have negative values in both Bias and MTS while failing parts will have a positive value in the Bias, MTS, or both.

CONCLUSIONS AND FUTURE WORK

This work demonstrates that a PCRT targeted defect sort is able to distinguish between modeled components with and without MTR volumes in the presence of expected process variations. The two VIPR sorts correctly sorted 95% of the components examined where ~44% of all missorted parts contained near-isotropic MTR's. Thus, the fast, objective, and automated detection of MTR's is feasible with PCRT methods.

The targeted PCRT sorting analyses presented here were performed on populations of modeled components generated using two generic disk geometries, Monte-Carlo style sampling, and realistic MTR's. FEM approximations of real MTR's were developed based on a publicly available dataset of MTR characteristics by randomly sampling the various MTR parameters. Statistically significant populations of components, with and without MTR volumes, were then generated and used to train a Pass/Fail defect sort targeting the MTR volumes.

One of the impediments to this work specifically and the field of MTR NDE generally was the lack of available literature regarding the characteristics of MTR's and their statistical occurrences in titanium aircraft components. The MTR models in this study are based off of a single dataset. Variations in the forging and forming processes will change the size, shape, orientation, and distribution of MTR's in a component. Another hindrance was the lack of a defined relationship between MTR parameters and the likelihood of crack initiation before the expected service life. The genetic algorithm employed by VIPR utilizes such severity metrics to optimize the detection of life-limiting features.

Verification of the models presented here is currently underway using real geometries with characterized MTR's. Future work includes utilizing model-based PCRT sorting solutions to detect MTR volumes in a population of real titanium gas turbine engine components. Topics for additional investigations include the development of an MTR severity metric and additional MTR characterization.

ACKNOWLEDGMENTS

This research was supported by the U.S. Air Force Research laboratory (AFRL) through a Materials and Manufacturing Directorate (AFRL/RX) Structural Materials Broad Agency Announcement (BAA) Contract FA8650-15-C-5208 and an AFRL Small Business Innovation Research (SBIR) Phase II Contract, FA8650-15-C-5074. This paper has been cleared for public release by AFRL under case number 88ABW-2018-5115. Our thanks to Adam Pilchak (AFRL) for useful discussions and technical insights, John Wertz (AFRL) for ultrasonic scans, and John Porter (UDRI) for logistical and data collection support.

REFERENCES

1. A. L. Pilchak, J. Shank, J. C. Tucker, S. Srivatsa, P. N. Fagin, and S. L. Semiatin, "A dataset for the development, verification, and validation of microstructure-sensitive process models for near-alpha titanium alloys," *Integrating Materials and Manufacturing Innovation*, Vol. 5, No. 14, pp. 1-18, (2016), <https://doi.org/10.1186/s40192-016-0056-1>.
2. Dataset Archived on the NIST repository: <http://hdl.handle.net/11256/647>
3. A. P. Woodfield, M. D. Gorman, J. A. Sutliff, R. R. Corderman, "Effect of Microstructure on Dwell Fatigue Behavior of Ti-6242," *Titanium '95: Science and Technology*, P. A. Blankinsop, W. J. Evans, and H. M. Flower, Eds., Institute of Materials, Birmingham, UK, pp. 1116-1123, (1996).
4. M. R. Bache, "A review of dwell sensitive fatigue in titanium alloys: the role of microstructure, texture and operating conditions, *International Journal of Fatigue*, Vol 25, pp. 1079-1087, (2003)
5. A. L. Pilchak, A. Bhattacharjee, R. E. A. Williams, J. C. Williams, "The Effect of Microstructure on Fatigue Crack Initiation in Ti-6Al-4V," Proceedings 12th International Conference on Fracture, pp. 1-10, (2009).
6. A. L. Pilchak, A. H. Rosenburger, K. Nakase, I. Inagaki, Y. Shirai, J. C. Williams, "The influence of microstructure and microtexture of fatigue crack initiation and growth in α + β titanium," *Proceedings 12th International Conference on Titanium*, L. Zhou, H. Chang, Y. Lu, and D. Xu, Eds., (2011)
7. C. J. Szczepanski, S. K. Jha, J. M. Larsen, J. W. Jones, "The role of microstructure on various stages of the very high cycle fatigue behavior of an α + β titanium alloy, Ti-6Al-2Sn-4Zr-6Mo," *Proceedings 5th International Conference on Very High Cycle Fatigue*, C. Berger, H.-J. Christ, Eds., (2011)
8. N. Gey, P. Bocher, E. Uta, L. Germain, M. Humbert, "Texture and microtexture variations in near-α titanium forged disk of bimodal microstructure," *Acta Materialia*, Vol 60, pp. 2647-2655, (2012).

9. A. M. Blankenship, *Elucidating the Role of Microstructure, Texture, and Microtexture on the Dwell Fatigue Response of Ti-6Al-4V*, MS Thesis, Wright State University, (2014)
10. A. L. Pilchak, "A simple model to account for the role of microtexture on fatigue and dwell fatigue lifetimes of titanium alloys," *Scripta Materialia*, Vol 74, pp. 68-71, (2014).
11. A. L. Pilchak, J. C. Tucker, T. J. Weihing, "Determining the Probability of Occurrence of Rarely Ocurring Microstructual Configuration for Titanium Dwell Fatigue," *From Microstructure to Multiscale Modeling*, D. Brancherie, P. Feissel, S. Bouvier, A. Ibrahimbegovic, Eds., John Wiley & Sons, Inc., Hoboken, NJ, pp. 41-64, (2017).
12. Schwarz, J., Saxton, J., and Jauriqui, L., "Process Compensated Resonant Testing in Manufacturing Process Control," *Material Evaluation*, 63 736-739, (July 2005).
13. Piotrowski, D., Hunter, L., and Sloan, T., "Process Compensated Resonance Testing JT8D-219 1st Stage Blades," *ATA NDT Forum 2008,* (2008). <http://www.vibrantndt.co.uk/files/2008_ATA_NDT_Forum-PCRT_of_JT8D-T1_Blades.pdf>.
14. D. M. Craig, "NDT Technology Readiness: A P&WC Case Study," *2016 Airlines for America NDT Forum*, (2016).
15. D. Piotrowski, G. Weaver, "Enhancing Reliability with Process Compensated Resonance Testing (PCRT) at Delta TechOps," *2016 Airlines for America NDT Forum*, (2016).
16. ASTM E2001-13, *Standard Guide for Resonant Ultrasound Spectroscopy for Defect Detection in Both Metallic and Non-metallic Parts*, ASTM International, West Conshohocken, PA, (2013).
17. ASTM E2534-15, *Standard Practice for Process Compensated Resonance Testing Via Swept Sine Input for Metallic and Non-Metallic Parts*, ASTM International, West Conshohocken, PA, (2015).
18. ASTM E3081-16, *Standard Practice for Outlier Screening Using Process Compensated Resonance Testing via Swept Sine Input for Metallic and Non-Metallic Parts*, ASTM International, West Conshohocken, PA, (2016).
19. E. Biedermann, J. Heffernan, A. Mayes, G. Gatewood, L. Jauriqui, B. Goodlet, and S. Mazdiyasni, "Process compensated resonance testing modeling for damage evolution and uncertainty quantification," *Proceedings of the 43rd Annual Review of Progress in QNDE*, D. E. Chimenti, L. J. Bond, Eds., p. 090005, (2017).
20. J. Heffernan, L. Jauriqui, E. Biedermann, A. Mayes, R. Livings, B. Goodlet, and S. Mazdiyasni, "Process compensated resonance testing models for quantification of creep damage in single crystal nickel-based superalloys," *Materials Evaluation*, 75, n 7, pp. 941-952, (2017).
21. J. Heffernan, E. Biedermann, A. Mayes, R. Livings, L. Jauriqui, B. Goodlet, J.C. Aldrin, S. Mazdiyasni, "Detection and Quantification of Creep Strain Using Process Compensated Resonance Testing (PCRT) Sorting Modules Trained with Modeled Resonance Spectra," *Proceedings of the 44th Annual Review of Progress in QNDE*, D.E. Chimenti, L. J. Bond, Eds., p. 14006, (2018).
22. A. Mayes, L. Jauriqui, E. Biedermann, J. Heffernan, R. Livings, J. C. Aldrin, B. Goodlet, and S. Mazdiyasni, "Part-to-itself (PTI) model inversion in process compensated resonance testing (PCRT)," *Proceedings of the 44th Annual Review of Progress in QNDE*, D.E. Chimenti, L. J. Bond, Eds., p. 14002, (2018).
23. J. Heffernan, E. Biedermann, A. Mayes, R. Livings, L. Jauriqui, S. Mazdiyasni, "Validation of Process Compensated Resonance Testing (PCRT) Sorting Modules Trained with Modeled Data," These proceedings.
24. A. Mayes, J. Heffernan, L. Jauriqui, R. Livings, e. Biedermann, J. C. Aldrin, S. Mazdiyasni, "PCRT Inversion for Material Characterization and Digital Twin Calibration," These proceedings.
25. Private communications with Dr. Adam Pilchak (AFRL), Dec. 2017 to present.
26. L. Yang, J. A. Turner, "Ultrasonic characterization of microstructure evolution during processing," *Journal of the Acoustical Society of America,* vol 121, no 1, pp. 50-59, (2007).
27. L. Yang, J. Li, O.I. Lobkis, S.I.Rokhlin, "Ultrasonic Propagation and Scattering in Duplex Microstructures with Application to Titanium Alloys," *Journal of Nondestructive Evaluation*, Vol. 31, pp. 270-283, (2012).
28. A. Kaushal, "Power Turbine Disc" CAD model, *Grabcad*, Cambridge, MA, (2012) <https://grabcad.com/library/single-stage-turbine-wheel-n-blades-1/details?folder_id=795360>.
29. G. Simmons and H. Wang, *Single Crystal Elastic Constants and Calculated Aggregate Properties: A Handbook*, The MIT Press, Cambridge, MA, (1971).
30. G. Taguchi, S. Chowdhury, *The Mahalanobis-Taguchi System*, McGraw-Hill Education, New York City, NY, (2001).
31. G. Taguchi, R. Jugulum, *The Mahalanobis-Taguchi Strategy: A Pattern Technology System*, John Wiley & Sons Inc., Hoboken, NJ, (2002).